www.sciencemag.org/cgi/content/full/science.aac8353/DC1

Supplementary Material for

Geomorphic and geologic controls of geohazards induced by Nepal's 2015 Gorkha earthquake

J. S. Kargel,* G. J. Leonard, D. H. Shugar,* U. K. Haritashya,* A. Bevington, E. J. Fielding, K. Fujita, M. Geertsema, E. S. Miles, J. Steiner, E. Anderson, S. Bajracharya, G. W. Bawden, D. F. Breashears, A. Byers, B. Collins, M. R. Dhital, A. Donnellan, T. L. Evans, M. L. Geai, M. T. Glasscoe, D. Green, D. R. Gurung, R. Heijenk, A. Hilborn, K. Hudnut, C. Huyck, W. W. Immerzeel, Jiang Liming, R. Jibson, A. Kääb, N. R. Khanal, D. Kirschbaum, P. D. A. Kraaijenbrink, D. Lamsal, Liu Shiyin, Lv Mingyang, D. McKinney, N. K. Nahirnick, Nan Zhuotong, S. Ojha, J. Olsenholler, T. H. Painter, M. Pleasants, Pratima KC, QI Yuan, B. H. Raup, D. Regmi, D. R. Rounce, A. Sakai, Shangguan Donghui, J. M. Shea, A. B. Shrestha, A. Shukla, D. Stumm, M. van der Kooij, K. Voss, Wang Xin, B. Weihs, D. Wolfe, Wu Lizong, Yao Xiaojun, M. R. Yoder, N. Young

*Corresponding author. Email: kargel@hwr.arizona.edu (J.S.K.); dshugar@uw.edu (D.H.S.); uharitashya1@udayton.edu (U.K.H.).

Published 17 December 2015 on *Science* Express
DOI: 10.1126/science.aac8353

This PDF file includes:

Materials and Methods
Figs. S1 to S6
Tables S1 to S3

MATERIALS AND METHODS

Geohazard inventory, mapping, and database

4,312 landslide locations were mapped by six analyst teams organized around six Areas of Interest (Fig. S1). Landslide single points primarily indicate the location of deposits. This stems from our primary humanitarian motivation to identify locations of possible river blockage and village destruction, which is more frequent in valleys and lower mountain elevations where deposits occur.

Table S1 lists the number and type of images that were available for this study and the number used. Many more images were evaluated with null results. Thousands of unused images are available for future evaluation of Gorkha earthquake-related geohazard chronologies. Many additional images in Google Earth were heavily utilized for validation/quality assessment. Images vary in properties and quality (spectral, spatial, temporal, and radiometric resolution; sensor gains and DN range; cloud cover; look angles; geometric correction, and orthorectification). Analysts used GIS or remote sensing software of their choosing to scan for co-seismic and post-seismic geohazard features and cross-checked them against pre-earthquake imagery. We expended considerable effort to minimize omissions, false positives, and redundancies, and to establish the chronology of landslide development. Google Earth's timeline was useful to screen out pre-seismic landslides and confirm likely co-seismic and post-seismic ones.

Ten days of aerial and ground investigations were undertaken over limited areas by a team led by author B. Collins (USGS); their helicopter traverses, incorporating guidance provided by the Volunteer Group, allowed verification and qualification of our data and interpretations. Author D. Breashears conducted independent reconnaissance and acquired some of the photos used here. The reconnaissance verified many satellite-mapped landslides but also indicated many small landslides that we had not identified mainly due to limited resolution.

Our first response to the earthquake was humanitarian in nature and had no relation to scientific inquiry; this changed only after the emergency had eased and we had accumulated a very interesting body of data. During the intense first weeks of our response, 2-hour teleconferences were held (daily for the first three weeks, then biweekly to weekly) among disaster response officials from NASA, USGS, USAID, and other U.S. agencies, and experts from academia (together, the Response Team). Subgroups formed, to which several authors belonged, to facilitate communication among experts in Earth surface deformation, induced hazards, satellite image tasking, and other emergency activities. Several authors took major roles with one or more working groups and the broader NASA-led response. Subgroups worked interactively, disseminated analysis results and received and distributed information produced by the volunteer analysts on sites of urgent concern.

Before the ad hoc structure had a chance to form, within about a day after the earthquake, information was passed from the Volunteers to NASA that Langtang Valley was in trouble and that other Himalayan valleys were likely also severely affected. This information led initially to focused satellite targeting, then blanket repeat imaging of the whole earthquake-affected mountain area of Nepal and neighboring countries. Specific tips also emanated from experts connected with classified satellite assets. A separate set of communication lines extended from the volunteer group to experts in Nepal (mainly at

ICIMOD and DHM), to local resident "citizen-scientists" who were able to help, and to the Prime Minister of Nepal. ICIMOD and NASA each issued a series of urgent press releases prepared by the volunteers that were aimed at calming the public where needed and otherwise provided information required by the public and emergency response officials. The press releases were vetted by NASA and/or ICIMOD, with input from DHM and Nepalese experts. Hence, there was a rapidly organized web of communications that worked surprisingly well, mainly due to the Volunteers' unselfish sharing of analysis results and willingness to work under exceptional emergency conditions, and due to end users' urgent need for information.

The volunteer teams' identification of landslides as co/post-seismic (vs. pre-seismic) was fairly reliable based on validation by the first four authors. Inter-operator and inter-sensor inconsistency may affect the numbers of missed or variably clustered small landslides. In future work, we expect that both cooperation with and competition amongst other research groups will produce improved databases and analysis results. As more satellite data becomes available, we expect that our database can be utilized to study detailed time-series of post-seismic landslide evolution.

For each landslide or geohazard identified, a set of attributes was recorded, including:

1. Hazard_ID: Latitude and longitude to three or four decimal places, and the date of the first identified satellite image to contain the feature (DDMMYYYY), formatted as: Lat.Lon.FirstDate.
2. Group_ID: Name of the AOI;
3. Lat_dd: Latitude to three (or four) decimal places;
4. Lon_dd: Longitude to three (or four) decimal places;
5. Country: Country in which the geohazard is located;
6. Npl_Adm4: Nepal administrative district, based on the Global Administrative Areas GIS shapefile (http://www.gadm.org/home).
7. Chn_Adm: China administrative district, based on the Global Administrative Areas GIS shapefile.
8. Village: Nearest village to be impacted (e.g. downstream of dammed lake), based on OpenStreetMap data (http://download.geofabrik.de/asia/nepal.html) or Google Earth, commonly Digital Globe imagery
9. Analyst: Name(s) of analysts who worked on the specific feature.
10. Image_post: Filename of first post-earthquake image to contain the feature. If more than one scene analyzed, all scene IDs recorded.
11. Image_post_dat: Date (DDMMYYYY) of earliest post-earthquake scene to contain feature.
12. Image_pre: Filename of latest pre-earthquake scene not containing feature.
13. Image_pre_dat: Date (DDMMYYYY) of latest pre-earthquake scene not containing feature.
14. Hazard_type: Qualitative description of the feature, either as avalanche, landslide, landslide complex, rock avalanche.
15. Reactivate: Qualitative determination of whether the post-earthquake feature was a reactivation of an earlier landslide. (yes/no)
16. Water_hzd: Qualitative description of whether the feature directly affects a waterway (yes/no).

17. Visib_dam: Qualitative description of whether a dam across a river is present (yes/no/partial).
18. New_water: Qualitative description of whether water has begun to pond upstream of a dam (yes/no).
19. Infra_hzd: Qualitative description of whether the feature directly affects infrastructure (yes/no).
20. Dat_qual: Qualitative description of the imagery quality (high/med/low).
21. Risk: subjective classification of the potential risk posed by the feature and follow-on hazards (low/med/high). Features flagged as 'high' were typically examined by other Lead Analysts for confirmation.
22. Descry_comm: Brief description of the hazard and/or additional comments.
23. Group_agency: Group identifier to maintain authorship in event of merged datasets ('NASA_ICIMOD_Volunteer').

Glacier lakes inventory, mapping, and database

The Nagoya University team of the Volunteer Group inspected images of 467 of Nepal's high altitude lakes for indications of GLOFs or landslide impacts and direct or delayed response to the Gorkha earthquake and aftershocks. An inventory compiled by Fujita et al. (*58*) was utilized as a guide allowing for the quick identification and study of lakes. The volunteer team acquired Worldview 1, 2, and 3 scenes (courtesy of Digital Globe) to manually evaluate GLOF risks for each lake from Mt. Makalu in the east to Mt. Annapurna in the west as originally inventoried by Fujita et al. (*58*), plus some lakes that are not in that inventory. Both pre-and post-earthquake images were inspected to identify possible changes in moraine structure and outlet channel width, signs of downstream flooding, increased number and size of icebergs in the lake, large cracks in the glacier terminus zone, lateral moraine collapse, moraine slumping, and other evidence of damage to the damming moraine, adjacent glacier, or adjoining mountainsides. A database was compiled, which characterized post-earthquake condition and a risk assessment for each lake. A second independent survey was conducted by a team of volunteer analysts from the University of Dayton. Their survey of several hundred lakes, consisting of mostly the same lakes as the Nagoya survey plus 24 additional lakes, found much the same results. A preliminary assessment of three of Nepal's most dangerous lakes was made based on Landsat 8 OLI, ASTER, and ALI images (Figs. 7B-J).

Earthquake-induced geohazard susceptibility index computation

Seismic and shake intensity data

Seismic data relating to earthquake and aftershock events, including epicenters, depths, time-of-event, and shake intensity were acquired from the USGS Earthquake Hazards Program (*35*) (Table S2). USGS ShakeMap data (Fig. 1B) are available in ASCII format and contain metrics of shake velocity and acceleration amplitudes posted at regularly spaced grid nodes (including peak ground acceleration, PGA, which we used in our analysis).

Topographic data and slope determination

Slopes were determined using Shuttle Radar Topography Mission (SRTM) 3-arc second (~90 meter) gap-filled DEMs available through the Consultative Group for International Agricultural Research, Consortium for Spatial Information (CGIAR-CSI) (*32*).

Generation of Hazards Susceptibility Indices

Gridded values of the seismically induced PGA, measured in percent *g* (gravitational acceleration), were collected for the local highest PGA for the primary M7.8 Gorkha earthquake and the subsequent five aftershocks > M6.0 up to the 12 May 2015 M7.3 aftershock (Table S2). Gridded PGA was converted to continuous raster format and posted on 2000 m cell spacing.

The shake zone covers 155,000 km^2, delineated by areas containing USGS PGA ≥ 0.03 *g*. Hazard susceptibility maps (Fig. 2) were computed across the shaken zone for each SRTM 90-m cell:

$$HazardSusceptibility = PGA_{MAX} * \left(\sin\left(Slope_{SRTM}\right)\right)$$

where PGA is from the USGS shake model (measured in fraction of *g*) and PGA_{MAX} is the largest PGA in each 2000-m grid cell for the six overlapping > M6.0 earthquakes and aftershocks. Slope is from the 90-m SRTM DEM. Table S3 summarizes the hazard susceptibilities for several landslides described in the Research Article. We calculated, normalized, and binned mass movement hazard susceptibility index values associated with i) ice avalanches, ii) snow avalanches, or iii) debris landslides.

The ice- and snow-dominated mass movement data are incomplete due to (i) difficult detection when avalanches are superposed over snow, (ii) short lifetimes when emplaced at low elevations, and (iii) problematic attribution of cause except where eyewitness reports are available. For example, the massive, deadly Everest ice/snow avalanches from 25 April 2015 are readily detected in WorldView scenes taken within days of the event, but had almost disappeared 4 weeks later.

PGA_{MAX} = 0.03 *g* is our threshold limit of concern based on the recognition that earthquake-induced ice avalanches occurred at PGA down to the levels near Mt Everest (~0.03-0.09 *g*), but not many mass movements occurred in less intensely shaken areas.

Land Cover Classification

<u>Glacier Ice</u> was extracted from version 4.0 of the Randolph Glacier Inventory *(34)*.

<u>Snow</u>: Two pre-earthquake Landsat-8 color-composite mosaics generated from mostly cloud-free 2013-2014 imagery were provided by the USGS EROS Data Center for the NASA-led Response Team: a band 543-RGB, and a band 432-RGB mosaic (30 meter resolution). A normalized difference snow index (NDSI) was generated from LS8 VNIR-SWIR bands 3, 6, and 8 (*Index = [B3 - B6] / [B3 + B6]*) and thresholded at ≥ 0.10, which classified most of the snow-cover. Some water and clouds, mis-classified as snow, were removed with an SRTM elevation mask to eliminate areas < 4580 m; a slope = 0 mask; filtering to remove snow areas < 0.002 km^2; and manual editing. Since the glacier ice fraction was also contained mainly within the broader snow-cover class, the RGI ice cover was subtracted from the snow area.

Land: All remaining area (not ice or snow) was classified as land.

Lithologic mapping

We followed a geological generalization and structural fault data from (*46, 47*).

Data integration and mapping properties

Multispectral imagery and DEMs were inspected for accurate co-registration; only one minor translational (XY) shift was required for Landsat 8 image bands and mosaics. Susceptibility index maps were resampled to 30 m and projected into a custom Albers equal area conic projection with a WGS 1984 datum.

Peak Ground Acceleration (PGA): artifacts, caveats, and alternatives

PGA is key in our landslide susceptibility analysis, but it is poorly constrained due to sparse intensity observations and lack of strong-motion measurements. USGS-computed ground motions were estimated primarily by Ground Motion Prediction Equations (GMPEs). Local sparse macroseismic reports/measurements ('did you feel it' shake reports) were integrated into the models. The USGS shake model for the main M7.8 shock may over-weight PGA locally, causing circular anomalies of high shaking within zones of moderate shaking. The model does not consider wave interactions with the topography and geologic structure, so local structure in PGA is not represented. Hence, the USGS ShakeMap has high regional and local uncertainties. Despite artifacts and lack of detail, we found PGA to be useful in assessment of landscape susceptibilities to mass movements. Considering the broad geographic coverage provided by the USGS ShakeMap, we used their model to compute shake-induced mass movement susceptibilities.

Noting the artifacts and limitations in the USGS ShakeMap, and aiming to develop better estimates of the extent and distribution of damage to buildings, fatalities, and rebuilding costs, researchers developed a preliminary inferred PGA map (*35*), which may be applied in future work. The inferred PGA over Nepal was determined by using observations of collapsed buildings from the National Geospatial-Intelligence Agency and building exposure estimates developed by ImageCat to determine the distribution of collapsed buildings. Composite damage functions were derived from USGS Pager collapse fragility functions (e.g., following *4*) and weighted by the structural distribution of building types for the region's various development patterns.

PGA probabilistic forecasts for future earthquakes, especially aftershocks, are straightforward and computationally tractable. Forecast and probabilistic ground motion intensity maps can be produced for postulated scenarios and ensemble models to show likely ground motions or damage (e.g., landslides) thresholds (e.g., *29*).

In sum, the modeling approaches are rooted alternatively in (i) pure geophysics amended by limited empirical observations (our adopted approach), (ii) inferences from observed and modeled damage, and (iii) probabilistic forecasts of future quakes and damage. In future work each approach will be informed and improved by the distribution of landslides.

Fatality distribution as an independent check of the USGS ShakeMap

The first fatality estimates for the Gorkha earthquake made by USGS relied on their ShakeMap (Fig. 1B), which we also used. Those death toll estimates were highly uncertain, initially indicating a 65% chance of fatalities ranging from 1,000 to 100,000. Ultimately, the death toll was in the middle, logarithmically. The main shock on 25 April killed 8,674 people in Nepal (including at least 164 foreigners), 130 in India, 27 in China, and 4 in Bangladesh. More than 99% of the deaths occurred in a 550 x 200 km swath, but scattered deaths occurred more widely across 1200 x 400 km. Subsequent aftershocks prior to 12 May killed 21 more in Nepal, and the giant 12 May aftershock killed an additional 163 in Nepal, 62 in India, 1 in China, and 2 in Bangladesh. At least 279 people remain missing. Fatality data were updated to 6 June 2015, collected from several sources, mainly a compilation by Earthquake-Report.com. About 99% of the total 9084 deaths from all the quakes and induced landslides occurred in a swath that roughly matches the east-west extent of the landslide distribution and the USGS ShakeMap (Fig. 1C); the correlation supports the use of the USGS ShakeMap, with due consideration of the caveats and potential improvements. Landslide-related deaths are partly connected with shake but also with slope, which is roughly anti-correlated with population density. Hence, the north-south extent of the high-density death distribution is different from the ShakeMap due to demographics, e.g., sparse populations in the higher Himalaya, and terrain slope properties.

Disclaimer

The views and interpretations in this publication are those of the authors. They are not necessarily attributable to any of the authors' institutions and do not imply the expression of any opinion by these institutions concerning the legal status of any country, territory, city or area of its authority, or concerning the delimitation of its frontiers or boundaries, or the endorsement of any product.

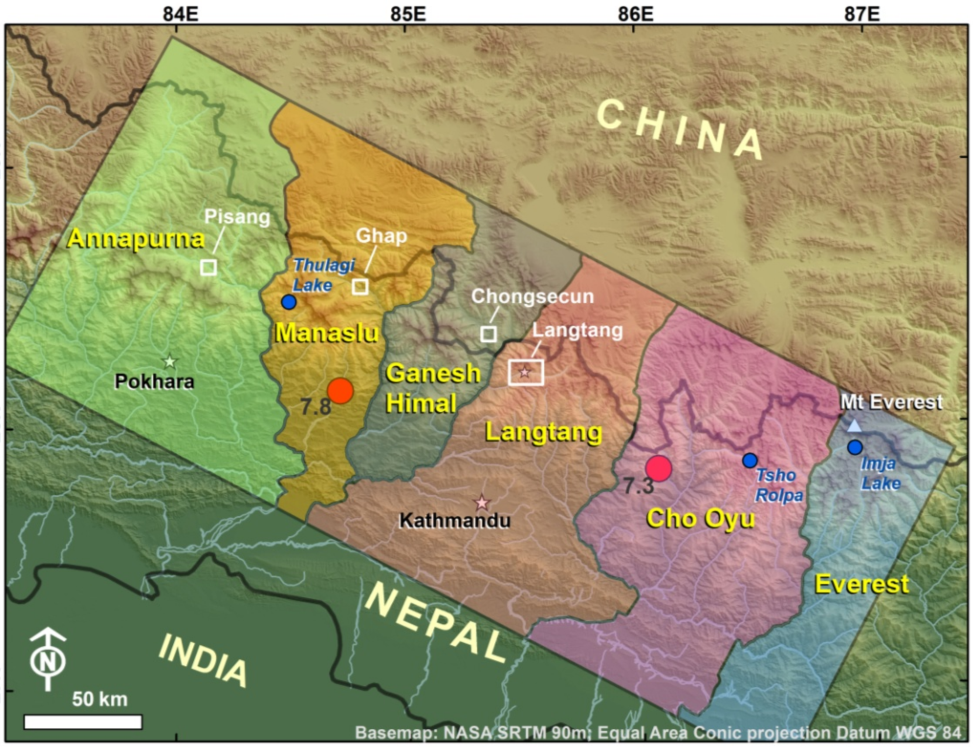

Fig. S1. Volunteer Image Analyst Group AOIs, locations of Case Study areas and glacier lakes described below, and epicenters of two largest earthquakes between 25 April - 30 May 2015.

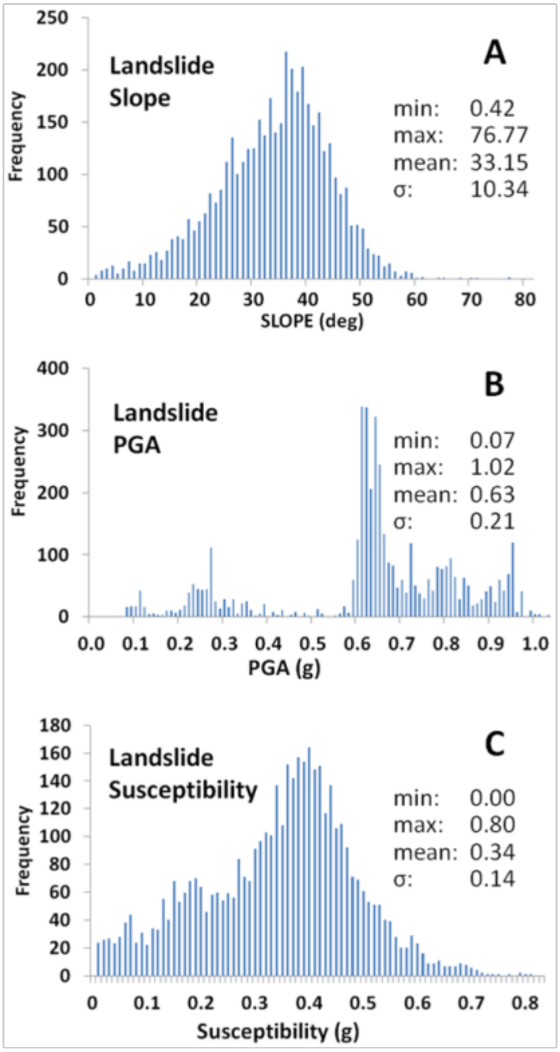

Fig. S2. Histograms of landslide occurrences. Landslides with respect to: (A) slope, (B) peak ground acceleration, and (C) landslide susceptibility index. All plots n = 4312.

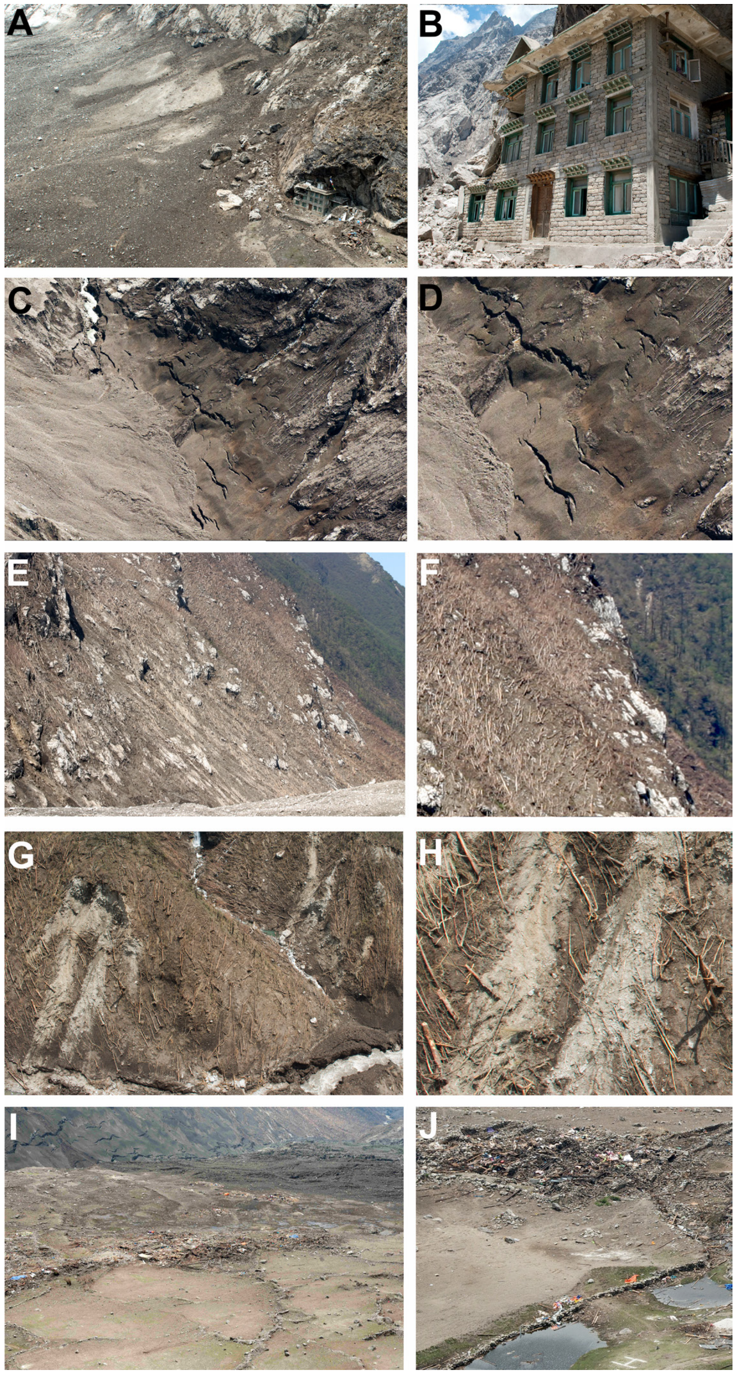

Fig. S3. Destroyed Langtang. (A) Proximal landslide deposit (the landslide head) against steep slopes on the north side of Langtang. The sole surviving structure in Langtang was protected by the cliff (lower right of panel A). (B) Sole surviving structure has typical stone-slab construction on a foundation. (C, D) Distal (toe) part of the landslide. The Langtang River (known locally as the Langtang Khola) has tunneled beneath the landslide. The deposit flowed onto landslide wind-deposited debris, which has formed crevasses due to slumping toward the river. (E,F) Forest of small trees flattened by a powerful blast of debris-laden, landslide-driven wind. (G,H) Small post-seismic landslide and the wind-flattened forest. (I,J) Completely demolished windblasted part of Langtang. Panels E and F by Randall Jibson. Others by D. Breashears (7 May 2015).

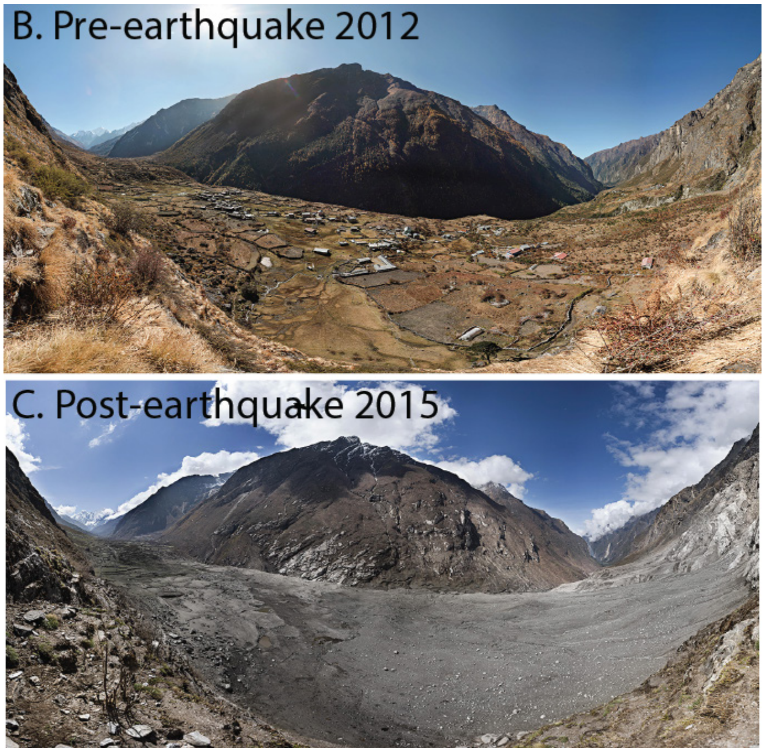

Fig. S4. Before and after photographs of Langtang Valley, showing burial and destruction of a large part of Langtang village. Photographs by D. Breashears.

Fig. S5. Extent of airblasts. West-facing aerial photo showing the extents of the air blast (dashed red line), the initial debris deposits and run-up (dashed purple line), and the secondary rockslide (dashed yellow line; photo 10 May 2015: D.F. Breashears/GlacierWorks).

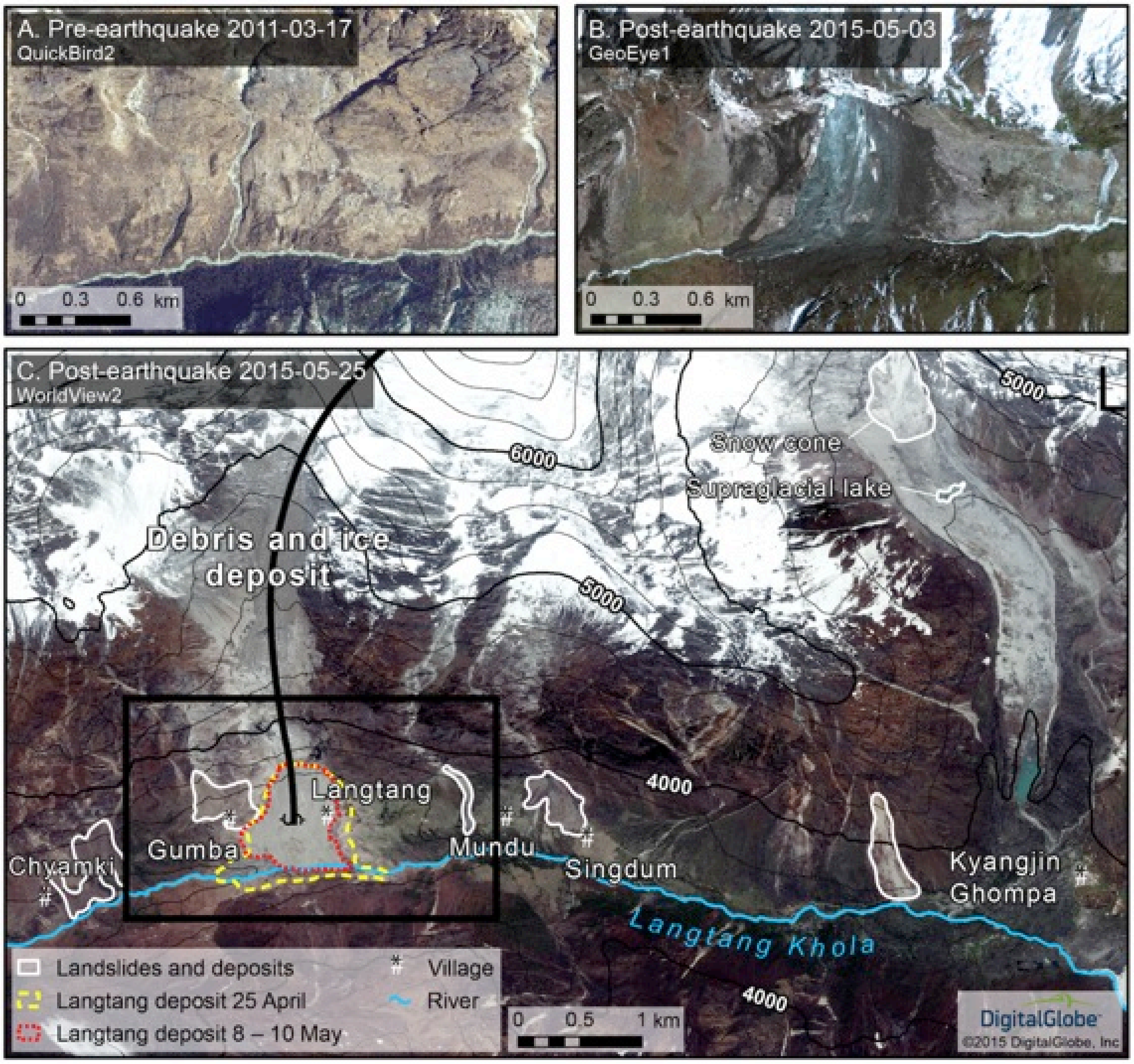

Fig. S6. Satellite images of the upper Langtang Valley. (A) Area of Langtang village prior to the earthquake on 17 March 2011. (B) Same area on 3 May 2015, after the earthquake. (C) Overview image/map of the upper Langtang Valley on 25 May 2015, annotated with a key avalanche flow route (black line). Images courtesy of Digital Globe.

Table S1. List of satellite sensors, platforms, and images used by and available to analysts for landslide analysis*

Period	Sensor/Product	Images Used	Images Available
Pre-earthquake	Gaofen-1	1	1
	EO1 ALI	2	2
	GeoEye 1	2	15
	Planet Labs	--	3091
	LANDSAT 7	1	1
	LANDSAT 8	9	30
	WorldView 1	2	21
	WorldView 2	9	163
	WorldView 3	3	18
	LANDSAT 8 Mosaic	2	2
	Totals	**31**	**3344**
Post-earthquake	EO1 ALI	4	32
	Planet Labs	--	7
	LANDSAT 7	3	10
	LANDSAT 8	6	68
	Terra ASTER	1	58
	WorldView 1	2	204
	WorldView 2	30	1066
	WorldView 3	4	561
	GeoEye 1	2	18
	Pleiades	--	1
	RADARSAT 2	--	2
	SPOT 6	--	4
	Totals	**52**	**2031**

* In addition, many of these same images, and a total of 7 WorldView 1, 60 WorldView 2, and 28 WorldView 3 images were used for the glacier lakes analysis.

Table S2. Primary earthquake and aftershocks (> M6), April 25 - May 12, 2015

USGS CUSP-ID	Mag	Epicentral Lat (dd)	Epicentral Lon (dd)	Date	Time (UTC)	W bound	S bound	E bound	N bound
us20002926	7.8	28.15	84.71	Apr-25 2015	06:11:26	81.7079	25.5013	87.7079	30.7933
us20002bi4	6.1	27.63	85.54	Apr-25 2015	06:15:22	82.5398	24.9705	88.5398	30.2865
us2000292y	6.6	28.19	84.86	Apr-25 2015	06:45:21	81.8645	25.5497	87.8645	30.8357
us200029bt	6.7	27.78	86.00	Apr-26 2015	07:09:10	82.9971	25.127	88.9971	30.437
us20002ejl	7.3	27.84	86.08	May-12 2015	07:05:19	83.0772	25.1848	89.0772	30.4888
us20002ek5	6.3	27.62	86.17	May-12 2015	07:36:53	83.1659	24.96	89.1659	30.276

USGS seismic data *(35)*

Table S3: Sample of induced hazard events, or nonevents, and their local earthquake influences

Location	Hazard Feature	Susceptibility Index (g)	PGA (% g)	Comment
Langtang, Nepal	landslide / air blast	0.05 - 0.20	25.8*	village completely destroyed (many casualties)
Pisang, Nepal	landslides	0.03 - 0.10	10.5-13.3	series of dammed lakes in Marsyangdi R.
Chongsecun, China	landslides	0.10 - 0.15	22.1	Dammed lake
Resuo Bridge	landslides	0.15 - 0.20	26.2	Roads blocked
Everest Base Camp	avalanche / air blast	0.03 - 0.08	9.5	Portion of BC destroyed (casualties)
Imja Lake, Nepal	none identified	NA	8.8	intact
Tsho Rolpa, Nepal	none identified	NA	18.2	Intact, but ground fractures on moraine dam
Thulagi Lake, Nepal	none identified	NA	22.7	intact
Unidentified small lake near Lhotse Glacier	Small outburst flood	NA	9.3	Small outburst flood (from supraglacial pond?) caused alarm but no damage

*represents only PGA values above the now demolished Langtang village; maximum values within the broader Langtang Valley are locally > 60% g.

References and Notes

1. R. M. Parameswaran, T. Natarajan, K. Rajendran, C. P. Rajendran, R. Mallick, M. Wood, H. C. Lekhak, Seismotectonics of the April–May 2015 Nepal earthquakes: An assessment based on the aftershock patterns, surface effects and deformational characteristics. *J. Asian Earth Sci.* **111**, 161–174 (2015). doi:10.1016/j.jseaes.2015.07.030

2. J. Galetzka, D. Melgar, J. F. Genrich, J. Geng, S. Owen, E. O. Lindsey, X. Xu, Y. Bock, J. P. Avouac, L. B. Adhikari, B. N. Upreti, B. Pratt-Sitaula, T. N. Bhattarai, B. P. Sitaula, A. Moore, K. W. Hudnut, W. Szeliga, J. Normandeau, M. Fend, M. Flouzat, L. Bollinger, P. Shrestha, B. Koirala, U. Gautam, M. Bhatterai, R. Gupta, T. Kandel, C. Timsina, S. N. Sapkota, S. Rajaure, N. Maharjan, Slip pulse and resonance of the Kathmandu basin during the 2015 Gorkha earthquake, Nepal. *Science* **349**, 1091–1095 (2015). Medline doi:10.1126/science.aac6383

3. E. O. Lindsey, R. Natsuaki, X. Xu, M. Shimada, M. Hashimoto, D. Melgar, D. T. Sandwell, Line-of-sight displacement from ALOS-2 interferometry: Mw7.8 Gorkha Earthquake and Mw7.3 aftershock. *Geophys. Res. Lett.* **42**, 6655–6661 (2015). doi:10.1002/2015GL065385

4. K. Jaiswal, D. Wald, D. D'Ayala, Developing empirical collapse fragility functions for global building types. *Earthq. Spectra* **27**, 775–795 (2011). doi:10.1193/1.3606398

5. J. S. Kargel, G. J. Leonard, M. P. Bishop, A. Kääb, B. H. Raup, *Global Land Ice Measurements from Space*. (Springer-Verlag, Berlin Heidelberg, 2014).

6. E. L. Harp, D. K. Keefer, H. P. Sato, H. Yagi, Landslide inventories: The essential part of seismic landslide hazard analyses. *Eng. Geol.* **122**, 9–21 (2011). doi:10.1016/j.enggeo.2010.06.013

7. J. A. N. van Aardt *et al*., Geospatial disaster response during the Haiti earthquake: A case study spanning airborne deployment, data collection, transfer, processing, and dissemination. *Photogramm. Eng. Remote Sensing* **77**, 943–952 (2011).

8. G. Cecchine *et al*., "The U.S. Military Response to the 2010 Haita Earthquake - Considerations for Army Leaders," (RAND Corporation, 2013).

9. H. P. Sato, E. L. Harp, Interpretation of earthquake-induced landslides triggered by the 12 May 2008, M7.9 Wenchuan earthquake in the Beichuan area, Sichuan Province, China using satellite imagery and Google Earth. *Landslides* **6**, 153–159 (2009). doi:10.1007/s10346-009-0147-6

10. British Geological Survey, Nepal earthquake response 2015 (available from http://www.bgs.ac.uk/research/earthHazards/epom/NepalEarthquakeResponse.html). (2015).

11. R. N. Parker, A. L. Densmore, N. J. Rosser, M. de Michele, Y. Li, R. Huang, S. Whadcoat, D. N. Petley, Mass wasting triggered by the 2008 Wenchuan earthquake is greater than orogenic growth. *Nat. Geosci.* **4**, 449–452 (2011). doi:10.1038/ngeo1154

12. C. Xu, X. Xu, X. Yao, F. Dai, Three (nearly) complete inventories of landslides triggered by the May 12, 2008 Wenchuan Mw 7.9 earthquake of China and their spatial distribution statistical analysis. *Landslides* **11**, 441–461 (2014). doi:10.1007/s10346-013-0404-6

13. R. M. Yuan, Q.-H. Deng, D. Cunningham, C. Xu, X.-W. Xu, C.-P. Chang, Density distribution of landslides triggered by the 2008 Wenchuan earthquake and their relationships to peak ground acceleration. *Bull. Seismol. Soc. Am.* **103**, 2344–2355 (2013). doi:10.1785/0120110233

14. E. L. Harp, R. W. Jibson, R. E. Kayen, D. K. Keefer, B. L. Sherrod, G. A. Carver, B. D. Collins, R. E. S. Moss, N. Sitar, Landslides and liquefaction triggered by the M 7.9 Denali Fault earthquake of 3 November 2002. *GSA Today* **13**, 4–10 (2003). doi:10.1130/1052-5173(2003)013<0004:LALTBT>2.0.CO;2

15. R. W. Jibson, E. L. Harp, W. Schulz, D. K. Keefer, Landslides triggered by the 2002 Denali fault, Alaska, earthquake and the inferred nature of the strong shaking. *Earthq. Spectra* **20**, 669–691 (2004). doi:10.1193/1.1778173

16. D. H. Shugar, J. J. Clague, The sedimentology and geomorphology of rock avalanche deposits on glaciers. *Sedimentology* **58**, 1762–1783 (2011). doi:10.1111/j.1365-3091.2011.01238.x

17. F. C. Dai, C. Xu, X. Yao, L. Xu, X. B. Tu, Q. M. Gong, Spatial distribution of landslides triggered by the 2008 Ms 8.0 Wenchuan earthquake, China. *J. Asian Earth Sci.* **40**, 883–895 (2011). doi:10.1016/j.jseaes.2010.04.010

18. D. H. Shugar, B. T. Rabus, J. J. Clague, D. M. Capps, The response of Black Rapids Glacier, Alaska, to the Denali earthquake rock avalanches. *J. Geophys. Res.* **117** (F1), F01006 (2012). doi:10.1029/2011JF002011

19. R. N. Parker, G. T. Hancox, D. N. Petley, C. I. Massey, A. L. Densmore, N. J. Rosser, Spatial distributions of earthquake-induced landslides and hillslope preconditioning in the northwest South Island, New Zealand. *Earth Surface Dynamics* **3**, 501–525 (2015). doi:10.5194/esurf-3-501-2015

20. S. G. Evans, O. V. Tutubalina, V. N. Drobyshev, S. S. Chernomorets, S. McDougall, D. A. Petrakov, O. Hungr, Catastrophic detachment and high-velocity long-runout flow of Kolka Glacier, Caucasus Mountains, Russia in 2002. *Geomorphology* **105**, 314–321 (2009). doi:10.1016/j.geomorph.2008.10.008

21. W. Haeberli, C. Huggel, A. Kääb, S. Zgraggen-Oswald, A. Polkvoj, I. Galushkin, I. Zotikov, N. Osokin, The Kolka-Karmadon rock/ice slide of 20 September 2002: An extraordinary event of historical dimensions in North Ossetia, Russian Caucasus. *J. Glaciol.* **50**, 533–546 (2004). doi:10.3189/172756504781829710

22. J. S. Kargel, G. Leonard, R. E. Crippen, K. B. Delaney, S. G. Evans, J. Schneider, Satellite monitoring of Pakistan's rockslide-dammed Lake Gojal. *Eos Trans. AGU* **91**, 394–395 (2010). doi:10.1029/2010EO430002

23. V. Vilímek, M. L. Zapata, J. Klimes, Z. Patzelt, N. Santillán, Influence of glacial retreat on natural hazards of the Palcacocha Lake area, Peru. *Landslides* **2**, 107–115 (2005). doi:10.1007/s10346-005-0052-6

24. M. Carey, Living and dying with glaciers: People's historical vulnerability to avalanches and outburst floods in Peru. *Global Planet. Change* **47**, 122–134 (2005). doi:10.1016/j.gloplacha.2004.10.007

25. S. A. Dunning, N. J. Rosser, D. N. Petley, C. R. Massey, Formation and failure of the Tsatichhu landslide dam, Bhutan. *Landslides* **3**, 107–113 (2006). doi:10.1007/s10346-005-0032-x

26. J. T. Weidinger, in *Natural and Artificial Rockslide Dams,* S. G. Evans, R. L. Hermanns, A. Strom, G. Scarascia-Mugnozza, Eds. (Springer, Berlin Heidelberg, 2011), pp. 243-277.

27. M. Geertsema, J. J. Clague, Pipeline routing in landslide-prone terrain. *Innovations* **15**, 17–21 (2011).

28. K. Hewitt, Disturbance regime landscapes: Mountain drainage systems interrupted by large rockslides. *Prog. Phys. Geogr.* **30**, 365–393 (2006). doi:10.1191/0309133306pp486ra

29. Materials and methods are available as supplementary materials on *Science* Online.

30. Y. Ogata, Statistical models for earthquake occurrences and residual analysis for point processes. *J. Am. Stat. Assoc.* **83**, 9–27 (1988). doi:10.1080/01621459.1988.10478560

31. D. K. Keefer, Investigating landslides caused by earthquakes - A historical review. *Surv. Geophys.* **23**, 473–510 (2002). doi:10.1023/A:1021274710840

32. C. Xu, X. Xu, J. B. H. Shyu, Database and spatial distribution of landslides triggered by the Lushan, China Mw 6.6 earthquake of 20 April 2013. *Geomorphology* **248**, 77–92 (2015). doi:10.1016/j.geomorph.2015.07.002

33. A. Jarvis, H. I. Reuter, A. Nelson, E. Guevara, Hole-filled seamless SRTM data v4 (available at http://srtm.csi.cgiar.org). (International Centre for Tropical Agriculture (CIAT), 2008).

34. P. Meunier, N. Hovius, J. A. Haines, Topographic site effects and the location of earthquake induced landslides. *Earth Planet. Sci. Lett.* **275**, 221–232 (2008). doi:10.1016/j.epsl.2008.07.020

35. H. T. Chou, C. F. Lee, S. C. Chen, in *Earthquake-Induced Landslides: Proceedings of the International Symposium on Earthquake-Induced Landslides,* K. Ugai, H. Yagi, A. Wakai, Eds. (2013), pp. 45-57.

36. L. Chen, X. Yuan, Z. Cao, L. Hou, R. Sun, L. Dong, W. Wang, F. Meng, H. Chen, Liquefaction macrophenomena in the great Wenchuan earthquake. *Earthq. Eng. Eng. Vib.* **8**, 219–229 (2009). doi:10.1007/s11803-009-9033-4

37. P. L. Moore, N. R. Iverson, D. Cohen, Ice flow across a warm-based/cold-based transition at a glacier margin. *Ann. Glaciol.* **50**, 1–8 (2009). doi:10.3189/172756409789624319

38. H. Blatter, G. K. C. Clarke, J. Colinge, Stress and velocity fields in glaciers: Part II. Sliding and basal stress distribution. *J. Glaciol.* **44**, 457–466 (1998).

39. N. Bo, J. Persson, in *Sliding on Ice and Snow: Physical Principles and Applications*. (Springer, Berlin, 1998), pp. 391.

40. J. T. Weidinger, Predesign, failure and displacement mechanisms of large rockslides in the Annapurna Himalayas, Nepal. *Eng. Geol.* **83**, 201–216 (2006). doi:10.1016/j.enggeo.2005.06.032

41. P. Deline *et al.*, in *Snow and Ice-Related Hazards, Risks and Disasters,* W. Haeberli, C. Whiteman, J. F. Shroder, Eds. (Elsevier, Amsterdam, 2015), pp. 521-561.

42. M. Geertsema, M. Chiarle, in *Treatise on Geomorphology,* J. F. Shroder, M. Stoffel, R. A. Marston, Eds. (Elsevier, Amsterdam, 2013), vol. 7: Mountain and Hillslope Geomorphology, pp. 217-222.

43. C. Liang, "Interferogram for ALOS2-track 48-swath ScanSARNominal14MHz; Feb 22, 2015 to May 3, 2015," UNAVCO InSAR Product, 10.7283/S2KW2R (2015).

44. R. W. Jibson, E. L. Harp, "Field reconnaissance report of landslides triggered by the January 12, 2010, Haiti earthquake," (U.S. Geological Survey Open-File Report 2011-1023, Reston, VA, 2011).

45. E. L. Harp, R. W. Jibson, Landslides triggered by the 1994 Northridge, California earthquake. *Bull. Seismol. Soc. Am.* **86**, S319–S332 (1996).

46. J. Stöcklin, Geology of Nepal and its regional frame: Thirty-third William Smith Lecture. *J. Geol. Soc. London* **137**, 1–34 (1980). doi:10.1144/gsjgs.137.1.0001

47. B. D. Collins, R. W. Jibson, "Assessment of existing and potential landslide hazards resulting from the April 25, 2015 Gorkha, Nepal earthquake sequence," (U.S. Geological Survey Open-File Report 2015-1142, Reston, VA, 2015).

48. J. P. McCalpin, E. W. Hart, "Ridge-top spreading features and relationship to earthquakes, San Gabriel Mountains region, Southern California - Part B: Paleoseismic investigations of ridge-top depressions," *Final Technical Report, Contract 1434-HQ-GR-1026, National Earthquake Hazards Reduction Program* (U.S. Geological Survey, 2002).

49. R. D. Nason, in *The San Fernando, California, earthquake of February 9, 1971, U.S. Geological Survey Professional Paper 733*. (U.S. Geological Survey, Washington, DC, 1971), pp. 97-98.

50. S.-J. Lee, D. Komatitsch, B.-S. Huang, J. Tromp, Effects of topography on seismic-wave propagation: An example from northern Taiwan. *Bull. Seismol. Soc. Am.* **99**, 314–325 (2009). doi:10.1785/0120080020

51. W. W. Immerzeel, L. Petersen, S. Ragettli, F. Pellicciotti, The importance of observed gradients of air temperature and precipitation for modeling runoff from a glacierized watershed in the Nepalese Himalayas. *Water Resour. Res.* **50**, 2212–2226 (2014). doi:10.1002/2013WR014506

52. K. Fujita, T. Nuimura, Spatially heterogeneous wastage of Himalayan glaciers. *Proc. Natl. Acad. Sci. U.S.A.* **108**, 14011–14014 (2011). Medline doi:10.1073/pnas.1106242108

53. S. Ragettli, F. Pellicciotti, W. W. Immerzeel, E. S. Miles, L. Petersen, M. Heynen, J. M. Shea, D. Stumm, S. Joshi, A. Shrestha, Unraveling the hydrology of a Himalayan catchment through integration of high resolution in situ data and remote sensing with an advanced simulation model. *Adv. Water Resour.* **78**, 94–111 (2015). doi:10.1016/j.advwatres.2015.01.013

54. C. Cadwalladr, Nepal earthquake: the village wiped off the map in a few terrifying seconds. (The Guardian, 2015).

55. ICIMOD, *Glacial Lakes and Glacial Lake Outburst Floods in Nepal*. (International Centre for Integrated Mountain Development, Kathmandu, Nepal, 2011), pp. 99.

56. J. J. Clague, S. G. Evans, A review of catastrophic drainage of moraine-dammed lakes in British Columbia. *Quat. Sci. Rev.* **19**, 1763–1783 (2000). doi:10.1016/S0277-3791(00)00090-1

57. K. Fujita, A. Sakai, S. Takenaka, T. Nuimura, A. B. Surazakov, T. Sawagaki, T. Yamanokuchi, Potential flood volume of Himalayan glacial lakes. *Nat. Hazards Earth Syst. Sci.* **13**, 1827–1839 (2013). doi:10.5194/nhess-13-1827-2013

58. S. Ma, R. J. Archuleta, M. T. Page, Effects of large-scale topography on ground motions as demonstrated by a study of the San Gabriel Mountains, Los Angeles, California. *Bull. Seismol. Soc. Am.* **97**, 2066–2079 (2007). doi:10.1785/0120070040

59. A. C. Byers, D. C. McKinney, E. A. Byers, "Post-earthquake assessment: Imja, Tsho Rolpa, and Thulagi glacial lakes in Nepal," (U.S. Agency for International Development, 2015).

60. W. Schwanghart, A. Bernhardt, A. Stolle, P. Hoelzmann, B. R. Adhikari, C. Andermann, S. Tofelde, S. Merchel, G. Rugel, M. Fort, Oliver Korup, Repeated catastrophic valley infill following medieval earthquakes in the Nepal Himalaya. *Science* (2015). 10.1126/science.aac9865

61. A. Arendt *et al*., "Randolph Glacier Inventory – A Dataset of Global Glacier Outlines: Version 4.0," (Global Land Ice Measurements from Space, Boulder, CO, 2014).

62. U.S. Geological Survey, Earthquake Hazards Program (available from http://earthquake.usgs.gov). (2015).

63. M. R. Dhital, *Geology of the Nepal Himalaya*. Regional Geology Reviews (Springer, 2015).

64. L. S. Walsh, A. J. Martin, T. P. Ojha, T. Fedenczuk, Correlations of fluvial knickzones with landslide dams, lithologic contacts, and faults in the southwestern Annapurna Range, central Nepalese Himalaya. *J. Geophys. Res.* **117** (F1), F01012 (2012). doi:10.1029/2011JF001984